THIOACETAMIDE AS A SULFUR PRECURSOR FOR CHALCOPYRITE THIN FILM SOLAR CELLS

by

ALEX ALPHONSE

Presented to the Faculty of the Graduate School of

The University of Texas at Arlington in Partial Fulfillment

of the Requirements

for the Degree of

MASTER OF SCIENCE IN MATERIALS SCEINCE AND ENGINEERING

THE UNIVERSITY OF TEXAS AT ARLINGTON

December 2009

ACKNOWLEDGEMENTS

I would like to thank Dr. Michael Jin, my very kind and witty thesis adviser for sharing his expertise and close supervision on my studies and experiment and for giving me an opportunity of doing research under his guidance.

I sincerely thank Dr.Pranesh Aswath for his support and for being my committee member. I would also like to thank Dr. Yaowu Hao for reviewing my thesis work and for being my committee member. I express my gratitude to all the professors and the department staff for offering their support whenever required, especially our secretary, Jennifer Standlee for helping me with ordering research supplies and helping me with my academic paperwork and also Libia who stood on my way for registering my course work.

I appreciate the help of Eduardo and Dennis from NanoFab who trained me on various equipments. I also would like to thank Dr. Jiechao Jiang and David for their support in using the characterization equipments at Characterization Center for Microbiology and Materials. Last but not least, I have to thank post- docs, Dr.Rajalakshmi Sundaramoorthy and Dr. Ki Hyun Kim, for their guidance in my research and helping me in difficult situations.

I appreciate the help of my colleagues and all the friends who motivated and supported me during my thesis work. I thank Chun young Lee who helped me in doing DSC and TGA analysis. I thank Emil, Bohoon, Eray, Vishwas, Hande, Rajesh Tummala and Fang for their consistent support during my entire student career.

Lastly, I would like to thank my brother Freeman Alphonse and my sister- in- law Beena Freeman and for their support and encouragement throughout the study. Also, I thank my Father Alphonse Arokiasamy and my mother Josphine Alphonse for their love and support in everything I have accomplished.

November 24, 2009

ABSTRACT

THIOACETAMIDE AS A SULFUR PRECURSOR FOR CHALCOPYRITE

THIN FILM SOLART CELLS

ALEX ALPHONSE, M.S

The University of Texas at Arlington, 2009

Supervising Professor: Michael Jin

Chalcopyrite $CuInS_2$ (CIS) thin films have the potential to be used in low cost terrestrial photovoltaic applications. The band gap of CIS is around 1.5 eV [1] and it well matches with the solar spectrum. However, the power conversion efficiencies in CIS solar cells are presently limited to 13.2% [2]. CIS absorber layers can be produced in a simple two-stage process consisting of the physical vapor deposition of a Cu-In bilayer – generally with Cu-rich composition - and its subsequent sulfurization under sulfur atmosphere made by either sulfur vapor or H_2S. While sulfur vapor is a safer option than H_2S for the sulfurization, gas-phase H_2S is believed to provide much more reliable sulfur atmosphere and preferable reaction chemistry potentially making better crystalline structure and also removing residue oxygen in the layer – it should be noted the best efficiency of 11.4 % has been achieved with sulfur vapor so far though [3]. Previously, H_2S and elemental sulphur were used as sources for sulphurization, but the stability and mobility of these sources are poor. This study has explored thioacetamide as a safer and more convenient source of sulfur for the sulfurization process. The thermal stability of thioacetamide has been investigated by differential scanning calorimetry and the decomposition temperature of thioacetamide was approximately 180°C. Upon decomposition, thioacetamide breaks down to H_2S and acetonitrile, and H_2S can be introduced into a sulfurization reactor. The

chalcopyrite CIS phase was confirmed by X-ray diffraction and it exhibits polycrystalline thin films, with a strong diffraction signature at (112) direction. Scanning electron micrographs of CIS thin-films show the evidence of grain growth towards copper rich films. Thioacetamide allows the use of H_2S during sulfurization process without having H_2S gas bottles to start with minimizing safety issues associated with the transportation and the installation of H_2S gas. Thioacetamide as a solid phase at room temperature also provides a very simple, low-cost sulfurization process configuration due to its stability.

TABLE OF CONTENTS

LIST OF ILLUSTRATIONS

LIST OF TABLES

CHAPTER 1

INTRODUCTION

This thesis presents a novel method for the sulphurization of Cu-In alloy metallic precursor thin-films using thioacetamide as a source of sulfur in order to make $CuInS_2$ (CIS) thin-films as a photovoltaic absorber.

Chalcopyrite thin-film solar cell represented by $Cu(In,Ga)Se_2$ (CIGS) is one of the most promising photovoltaic (PV) technologies as a single-junction CIGS solar cell has demonstrated a very high power conversion efficiency (PCE) of about 20 % [4], which proves that it can start compete with widely-used crystalline silicon (Si) solar cell technology. While the bandgap of CIGS is about 1.3 eV being optimum for the maximum harvesting of sunlight, CIS is also very important in studying high bandgap chalcopyrite solar cells to achieve highly efficient multijunction solar cells ultimately. The best PCE obtained for CIS solar cell is only about 12 % even though simple thermodynamic calculation based on its bandgap of 1.5 eV provides the upper limit of about 28.5 % [5].

Chalcogenizing the Cu-In/Ga alloy metallic precursor thin film under S, Se, or Te atmosphere to make a targeted chalcopyrite thin-film has been the leading production method in the industry due to its simplicity and low cost, which is adequate for solar cell manufacturing. The choice of a safe chalcogen source becomes an important question due to the toxicity of commonly used H_2S/H_2Se for the process. Thioacetamide which contains sulfur, is stable under standard storage condition, and can provide a necessary reaction with the metallic precursor layer to form semiconducting, chalcopyrite sulfide thin-films. This study will examine the thermal properties of thioacetamide, optimize experimental conditions to obtain chalcopyrite phase of CIS, study phase transformation upon sulfurization, and analyze the material properties of CIS thin-films made.

CHAPTER 2

BACKGROUND

There is a strong demand for renewable energies due to the limited availability of fossil and nuclear fuels and due to growing environmental problems. Photovoltaic energy conversion has the potential to contribute significantly to the electrical energy generation in the future. Currently, the cost for photovoltaic systems is one of the main obstacles preventing production and application on a large scale. A substantial decrease in production costs for modules, and therefore in overall system cost, is expected from the development of thin film solar cells. This is the background for the strong research interest in materials suitable for thin film solar cells like amorphous silicon, CdTe,Cu(In,Ga)Se_2 and $CuInS_2$.

2.1 Bulk-based vs Thin-Film Solar Cells

Nowadays, solar industry is exponentially growing, but the most challenging barrier in the market is to reduce the cost of the PV system. 90 % of the current market is occupied by conventional wafer-based (bulk-based) mono/multi-crystalline Si solar cells. Meanwhile, thin-film solar cell technologies represented by amorphous silicon, CdTe, and CIGS materials have made an eye-catching progress posing themselves as near-future competitors of the Si technology. For example, it is a remarkable achievement that First Solar from the United States got recently succeeded to produce a solar module for less than $1/watt by employing a process with a very fast run time - CdTe thin film absorber can be deposited with a rate of the order of μm/min in a mass-production configuration [6]. Other cost-cutting innovations are also emerging in the field. They include various types of solution processes such as spray deposition, nanoparticle-based printing, and liquid precursor-derived deposition. However, these solution-based niche technologies will potentially experience a shallow learning curve.

The following sections will present the general attributes of the thin-film solar cell materials comparing with the bulk-based Si solar cell technology and provide the comprehensive introduction of CIGS thin-film technology. The introduction will also survey the various chalcogen sources used in CIGS thin-film processes. At the end, the current understanding of the phase transformation of Cu/In metallic precursor layer into CIS phase will be given to support the discussion of experimental results in this study.

Bulk-based solar cell has a great share in the PV industry producing cells and modules based on mono- and multicrystalline wafer technology. Even the metallurgical-grade Si wafers obtained at a relatively cheaper price proved favorable for the PV industry, as they led to a reasonable efficiency - average PCE over 15 % [7]. High PCE and good stability are two essential requirements for any technology to be successful and the Si solar cell technologies have met them successfully. However, Si wafers are fragile, the size of individual solar cell is limited by the wafer size, and the high-power solar modules are bulky, heavy, and rigid making it inconvenient to transport, handle and install. Above all, crystalline Si has a low absorption coefficient (in the order of 10^3 cm^{-1}) due to its indirect band gap, which requires about 300 μm thick material for effective solar absorption unless extra optical enhancement techniques are used to increase optical path compensating the intrinsically low absorbing nature. Furthermore, the high cost of crystalline silicon wafers - they make up 40 ~ 50 % of the cost of a finished solar module - has led the industry to look for cheaper materials to make solar cells [8].

Thin-film solar cells[9] have great potential for cost reduction among the different photovoltaic technologies. Thin-film solar modules are made by depositing micrometer thick layers of photosensitive semiconducting materials on substrates such as glass, plastic or stainless steel. They consume far less material than bulk based solar cells and offer possibilities for large-scale PV manufacture and their smooth visual appearance is an advantage considering applications in building integration. The production phase is already showing improvements that will eventually be reflected in lower manufacturing costs - higher automation, fewer processing steps, and a simpler manufacturing technology facilitate the

production of the low-cost, large-area modules demonstrated by First Solar, MiaSole, Global Solar, NanoSolar, Solyndra and others.

The thin-film absorbers have high-absorption coefficient (~10^5 cm^{-1}), which is about 100 times higher than the Si wafer (Fig. 3.1). Thus about 1 ~ 2 μm of material thickness is sufficient to harness more than 90 % of the incident solar light. The high absorption coefficient helps in reducing the material mass significantly to make modules cost-effective. In addition, the monolithic integration – the interconnection of cells during thin-film depositions without the need of string them physically, allows producing large-area modules in the order of m^2 very effectively. Furthermore, the roll-to-roll manufacturing of flexible solar modules is possible by depositing films on flexible substrates and these flexible and lightweight solar cells (modules) facilitate several attractive applications. In turn, this gives high throughput and thus can reduce the energy payback time significantly.

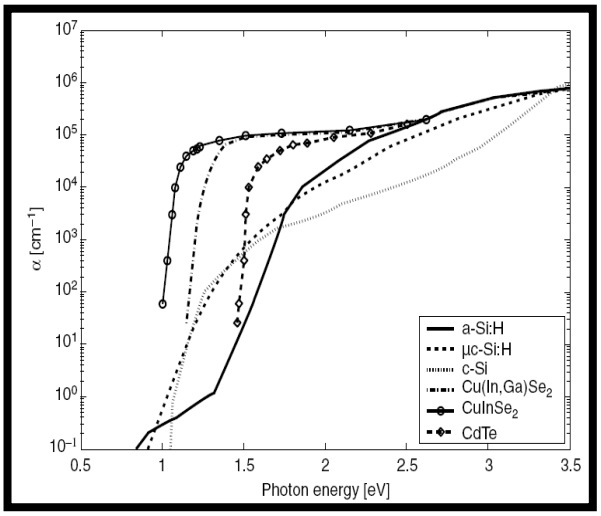

Fig 2.1 Photon energy vs. absorption coefficients of semiconducting materials [9]

2.2 Chalcopyrite Thin-Film Solar Cells

Compound semiconductors from the I–III–VI_2 series of the periodic table, such as $CuInSe_2$ (CISe), $CuGaSe_2$ (CGS), CIGS are often simply referred to as chalcopyrite because of their tetragonal crystal structure [10]. CIGS solar cell is most widely fabricated due to its

superior performance among various chalcopyrites. The bandgap of CISe is about 1.04 eV and the addition of Ga increases the band gap. The benefit of typical 20 ~ 30 at% Ga provides not only the better bandgap match to the solar spectrum but also the improved electronic quality of CIGS compared to CISe [10]. Either p-type or n-type CIGS can be prepared by making the film Cu-poor (Cu/In < 1) and Se-deficient respectively [11]. Cu vacancies are known to act as acceptors in CIGS, whereas Se vacancies act as donors [12]. Recently, the world best PCE for CIGS was set at about 20 % by National Renewable Energy Laboratory (NREL) [13, 14].

CIGS Solar-Cell Configuration: In the substrate configuration of CIGS solar cell (Fig. 2.2) [15], there are five different layers deposited typically on the glass substrate.

Back contact: The preparation of CIGS solar cells starts from deposition of molybdenum (Mo), which is a back contact. The properties of the Mo film and the choice of glass substrate are very important in solar cell applications. Usually Mo is sputtered on soda lime glass (SLG) substrate. Incorporation of sodium from the glass substrate into the CIGS absorber will passivate Se vacancies and provide a bigger composition (Cu/In ratio) window to form a stable chalcopyrite phase [16-18]. In most cases, $MoSe_2$ will form at the interface between Mo and CIGS on top. $MoSe_2$ is a p-type semiconductor and its band gap is larger than that CIGS providing a low recombination back surface for the photo-generated minority carriers in the CIGS absorber and at the same time it provides an ohmic contact for an easy collection of holes.

CIGS absorber layer: Because of a high absorption coefficient, a 2 μm-thick layer is sufficient for optimum absorption. While CIGS layers can be grown with a variety of deposition methods, leading manufacturing method is selenizing the stacked metallic layer under Se atmosphere as explained previously. It also needs to be noted that the 20 % efficient cell made by NREL was fabricated by thermal coevaporation - four elements were thermally evaporated in a vacuum chamber onto a heated substrate where a CIGS thin-film formed. Although the grain size, morphology, and surface roughness depend on deposition methods, efficiencies greater than 13% have been achieved with most of the methods. It has been revealed that the grain

boundaries in CIGS are benign – a low recombination velocity at the grain boundary either due to the passivation of defects by oxygen or relaxation of the grain boundary structure avoiding high density of states in its sub-bandgap energy. High-efficiency cells have been made with a p-type CIGS layer and an ordered defect compound, $CuIn_3Se_5$ phase on the surface of CIGS is believed to provide low recombination at the interface between absorber and the junction partner on top.

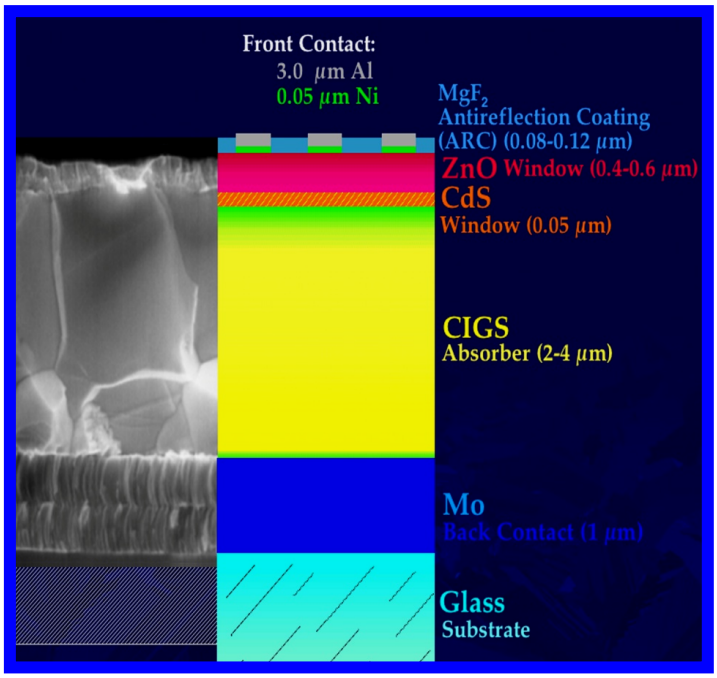

Fig 2.2 Basic layer structure of CdS/CIGS heterojunction solar cell [15]

Buffer Layer: The n-type buffer layer is deposited on top of CIGS. Typical buffer layer should have a large band gap of 2 ~ 3.5 eV, since it has to let solar spectrum to pass through to reach the CIGS absorber layer as much as possible. There are different types of buffer layers including CdS, ZnS(O,OH), In_2S_3, and ZnS [17-19]. While most highly efficient CIGS solar cells have CdS as a buffer layer, other alternatives have been sought in order to avoid the toxicity of Cd. The most common way to deposit CdS is by chemical bath deposition (CBD). Previously, the deposition of buffer layer was also done by physical vapor deposition such as sputtering, but

the efficiency of the cell was not good possibly due to the damage at the junction made during sputter deposition. Other deposition methods including metal organic chemical vapor deposition, atomic layer deposition, and a novel technique called ion layer gas reaction have been explored in the field [20]. Yet, most industries are currently using CBD-deposited CdS because of its conformal coating and low cost [20].

Window layer: Typical window layer includes doped ZnO or indium tin oxide. Usually, window layer has the band gap of around 3 eV transmitting 90% of the light. Nowadays, most research employs an aluminum-doped ZnO layer. Typically thin intrinsic ZnO layer is deposited prior to the doped ZnO in order to minimize the shunting in the cell.

Top contacts: A Ni/Al double layer is often deposited by evaporation as a top contact. Al often has an adhesion problem to CIGS and Ni is deposited before Al to help the adhesion.

2.3 Chalcogen Sources

This section reviews different types of chalcogen sources used for sulphurization or selenization and their merits and demerits. For example, elemental sulfur has been used in fabricating commercial modules by sulfurizing metallic precursor thin-films. It is solid at room temperature and it melts at about 120 ~ 150 ºC. It can provide high vapor pressure at above 150 $^{\circ}$C. Elemental selenium is also solid at room temperature and can produce vapor at elevated temperature. However, it is more toxic than sulfur [21]. Elemental chalcogen is also used in co-evaporation process. One inconvenience of using the elemental chalcogens is that it can condense very easily into any cold surface creating various maintenance problems. Another common chalcogen sources used in the chalcogenization process are H_2Se and H_2S. They are gas phases at room temperature and H_2Se is very toxic with the time-weighted average threshold limit value of 50 parts per billion and it should be stored in high pressure (20 Kgf/cm^2) cylinders [22]. Handling and storing the bottle of H_2Se can be very risky when compared to elemental source. According to National Federation of Paralegal Associations, the

health ratings for H_2Se is following - Health 4, Flammability 4, and Reactivity 4. Positively, the gas-phase hydride sources can effectively remove oxygen contamination in the CIGS film which can occur during the growth of chalcopyrite structure.

Thioacetamide: Due to the various demerits of using elemental chalcogen and chalcogen hydride sources in the chalcogenization of Cu-In/Ga metallic layer, it is necessary to seek a chalcogen source, which is reliable and risk-free in handling and transporting from one place to another in particular. Sulfurization of the surface of CIGS using an aqueous solution of thioacetamide was briefly introduced previously in order to widen the bandgap at the junction reducing recombination [23]. It has been known that thioacetamide decomposes in either acidic or basic water releasing H_2S – small amount of H_2S can be dissolved in water as well. As a result, the overall output characteristics of the CIGS solar cell was improved increasing PCE, which, in fact, has motivated author's study of using thioacetamide as a source of sulfur in sulfurizing Cu-In alloy metallic layer. It has been known that thioacetamide is white solid at room temperature and its melting point is around 114 $^{\circ}$C. Before reaching boiling, it thermally decomposes to H_2S and acetonitirile. Thioacetamide allows the use of H_2S during sulfurization process without having H_2S gas bottles to start with minimizing safety issues associated with the transportation and the installation of H_2S gas in the laboratory, which can provide a very simple, low cost sulfurization process.

2.4 Phase Transformation in the formation of Copper-Indium metallic layer

In order to understand the thermodynamics and kinetics of chalcogenization process of metallic layer, it is first necessary to understand how the metallic alloy layer forms during its PVD process and how they transform upon thermal annealing. For the Cu-In binary system, there have been three most commonly observed Cu-In alloy films at room temperature with the compositional range of about 50 at% In. They include $Cu_{11}In_9$, $CuIn_2$ and $Cu_{16}In_9$. According to the Cu-In phase diagram [24] (Fig. 2.3), $Cu_{11}In_9$ is stable up to about 310 ℃ and $C_{16}In_9$ phase (η) is stable up to about 383 ℃. The η' phase is not clearly defined, and various researchers

have proposed different phases including Cu_2In and Cu_7In_4 [25-28]. In addition, phase behavior of thin films of Cu-In alloys at 200℃ were addressed [29] and confirmed the presence of $Cu_{11}In_9$, CuIn, and an "undetermined phase" by comparing room temperature X-ray data [30] with JCPDS (Joint Council for Powder Diffraction Studies) card files. However, the samples in that study were not quenched and were allowed to cool in an uncontrolled environment which might have affected the results.

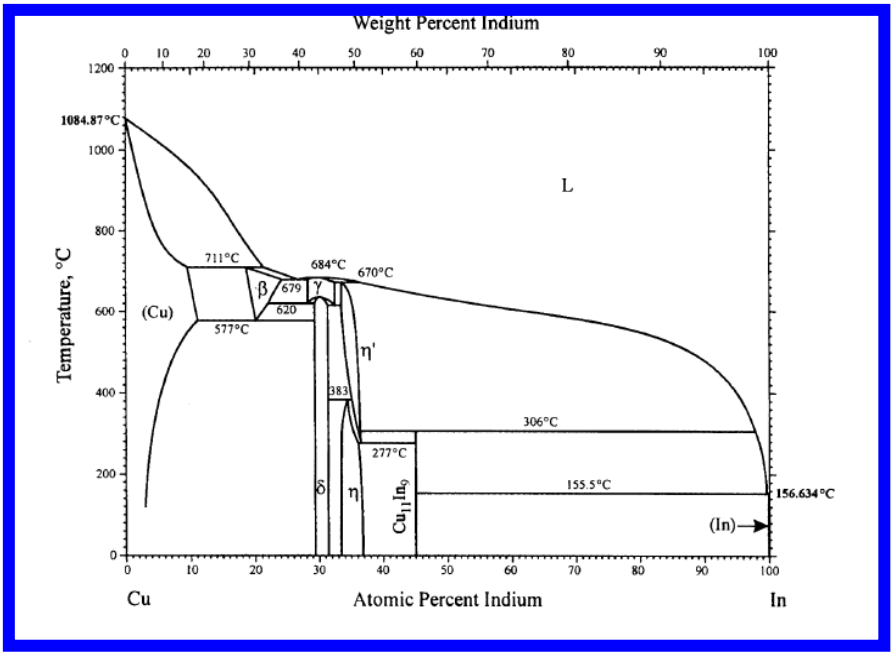

Fig 2.3 Cu-In phase diagram [24].

The following three subsections will elaborate on the three commonly observed Cu/In alloy phases observed from Cu/In bilayer deposited by PVD.

2.4.1 $CuIn_2$ phase

The $CuIn_2$ phase was discovered by Keppner [31] and the results from perturbed angular correlation confirmed that the Cu-In bilayer is stable only below 33°C. Above this temperature, the diffusion of Cu into In via interstitial sites sets in and leads to the formation of the In-rich phase, $CuIn_2$. Above 148 °C, $CuIn_2$ is no longer stable. The crystal lattice structure of $CuIn_2$ to

be compatible with that of $AgIn_2$ (Al_2Cu type) which has a tetragonal structure. The study showed that $CuIn_2$ is a bulk equilibrium phase of the Cu-In system although typical phase diagram does not show the phase and it can be produced in the Cu-In films deposited by thermal evaporation and sputtering.

2.4.2 $Cu_{11}In_9$ phase

$Cu_{11}In_9$ is formed from the peritectic reaction at around 307 $^{\circ}$C and the peritectic composition is 45 at% In. It has monoclinic crystal structure.

2.4.3 $Cu_{16}In_9$ phase

Depending on the composition, the $Cu_{16}In_9$ compound undergoes a phase transition from η-η' between 307 $^{\circ}$C and 389 $^{\circ}$C. The η' phase ($Cu_{16}In_9$) structurally differs from η and it coexists with liquid phase at peritectic reaction to form $Cu_{11}In_9$. The Cu–In phase diagram in the $Cu_{16}In_9$ region has been investigated extensively in the past. On looking at the phase diagram, we can confirm that the η' phase has an In composition of around 33 to 38% [32]. It confirms the stability of η' phase even at high temperature of around 671 $^{\circ}$C.

2.4.4 In-situ phase transition study on Cu-In alloy thin-films

Real-time transformation of the Cu-In alloy thin film upon thermal annealing with maximum temperature at 500 °C has been previously studied using energy dispersive X-ray diffraction (EDXRD) [33]. The characteristic EDXRD spectra obtained during the annealing of Cu-poor layer (Cu/In = 0.7) and Cu-rich layer (Cu/In = 1.8) are shown in Figs. 2.4 and 2.5 respectively.

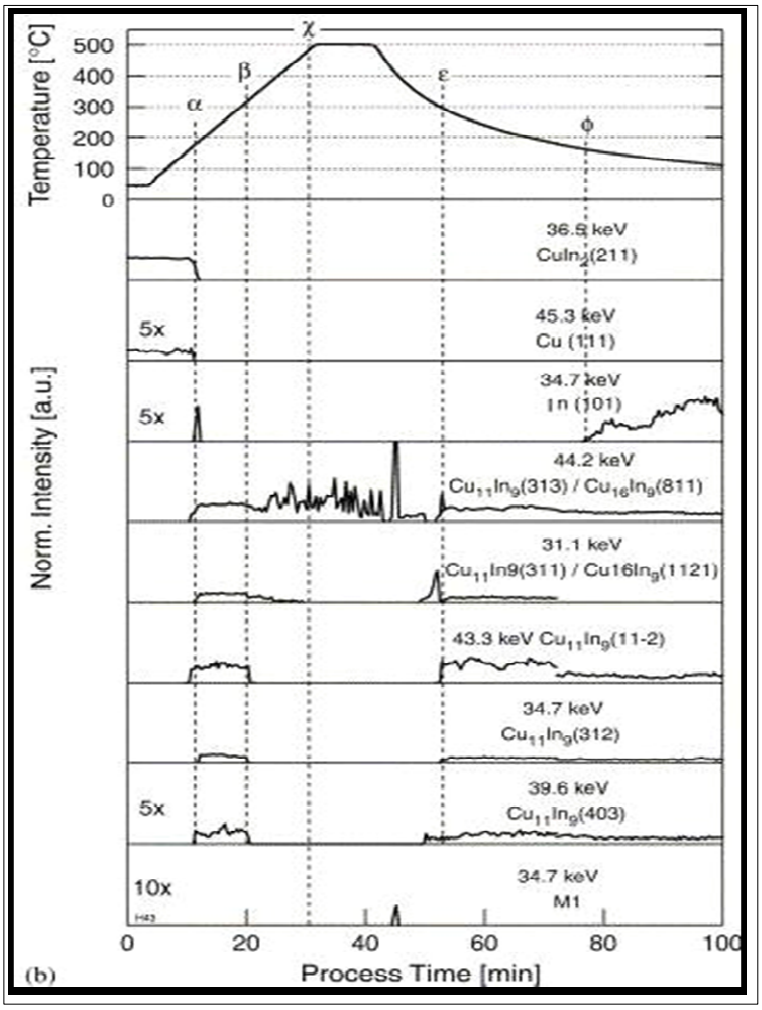

Fig 2.4 In-situ energy dispersive X-ray diffraction spectra: vacuum annealing of Cu-poor alloy layer (Cu/In = 0.7) [33].

As shown in Fig. 2.4, the Cu-poor alloy film contains $CuIn_2$ and a small amount of elemental Cu before annealing. When a temperature was reached at around 150 ℃ (marked as α in the plot), the $CuIn_2$ and Cu phases have disappeared and the characteristic $Cu_{11}In_9$ and In peaks appeared in the spectra. While $Cu_{11}In_9$ phase stayed longer, the In phase has disappeared quickly. This can be seen in Fig. 2.3 –at the given composition, the mixture of $Cu_{11}In_9$ and In is stable up to about 155 ℃ and it changes to the mixture of $Cu_{11}In_9$ and liquid phase with the further increase in temperature. While it was not easy to distinguish the diffractions of $Cu_{11}In_9$ and $Cu_{16}In_9$, the formation of $Cu_{16}In_9$ phase at higher temperature is expected from the Cu-In phase diagram and some of the diffractions from $Cu_{11}In_9$ have disappeared at around 300 ℃, which is again consis tent with the phase diagram. Overall

amount of solid phase continued decreasing as temperature increases and stayed high because liquidus line had a negative slope. During the cooling period, $Cu_{11}In_9$ peaks have reappeared at around 300 °C.

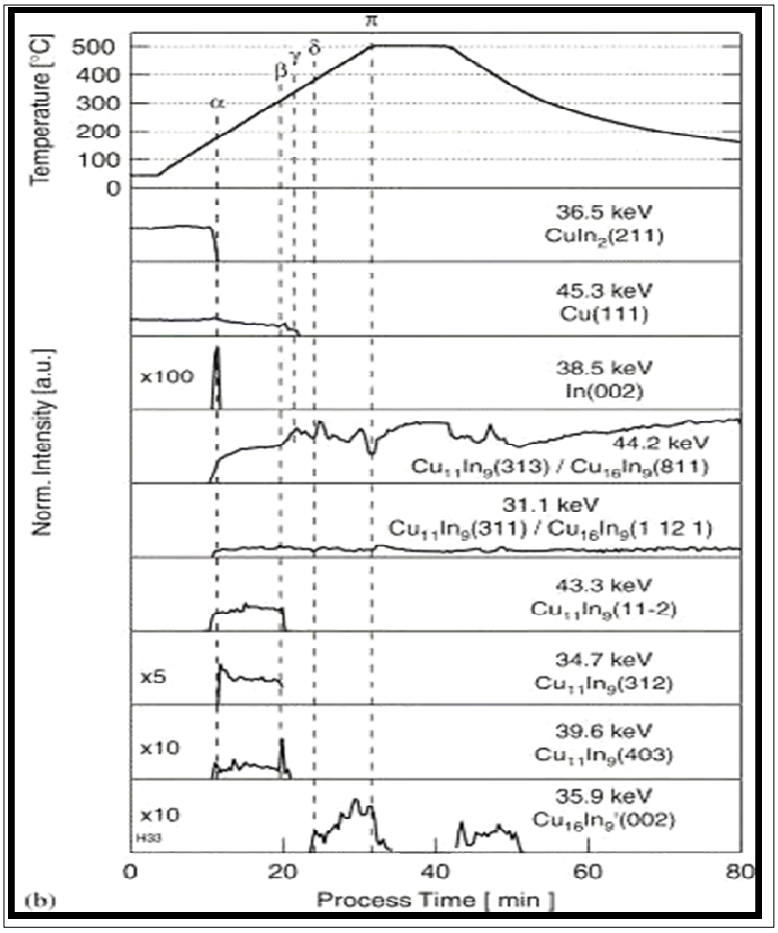

Fig 2.5 In-situ energy dispersive X-ray diffraction spectra: vacuum annealing of Cu-rich alloy layer (Cu/In = 1.8) [33].

The similar analysis can be made for the Cu-rich alloy film (Fig. 2.5). It is first interesting to see the phases existed before annealing were again $CuIn_2$ and Cu as seen in the Cu-poor composition. This can be rationalized though because the elemental Cu was indeed a substantial part of the starting sample this time. Again, the formation of $Cu_{11}In_9$ was observed above about 150 °C even though the overall composition does not predict its formation from the phase diagram. Possibly, the In-rich phase present in the beginning ($CuIn_2$) transformed

through $Cu_{11}In_9$ kinetically to reach equilibrium phase. As a result, the brief formation of the solid In phase has also been seen. The existence of η- $Cu_{16}In_9$ phase is again expected and there was clear indication of η′- $Cu_{16}In_9$ phase formation above about 380 ℃ this time – diffraction at 35.9 keV. Accordingly, the reverse phase transformation occurred at about 380 ℃ during cooling process and η′- $Cu_{16}In_9$ phase has disappeared.

2.5 Phase Transformation in $CuInS_2$

2.5.1 Phase diagram of Cu-In-S

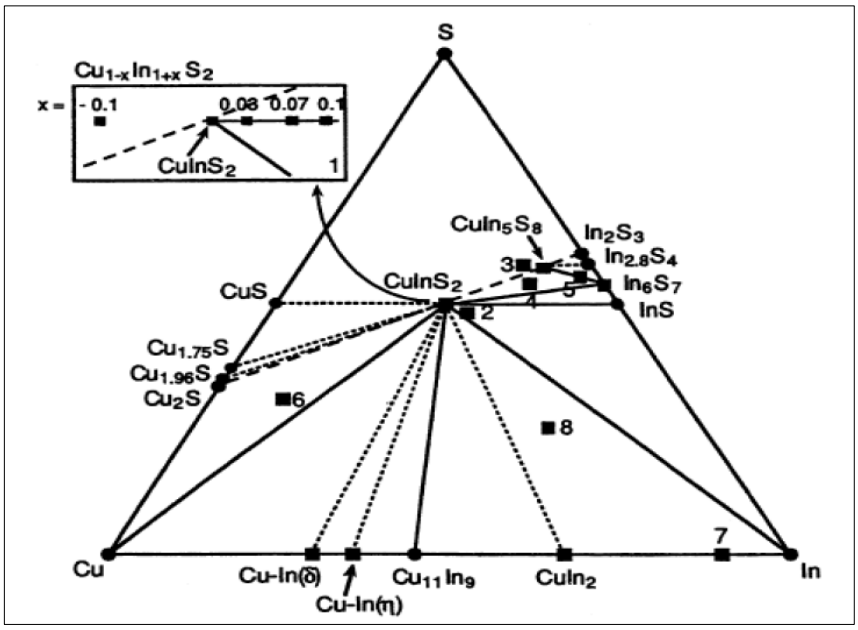

Fig 2.6 Ternary phase diagram of Cu-In-S [18].

The phase diagram of CIS is shown in Fig. 2.6 [18]. Many experiments have been conducted to study the formation of chalcopyrite compound and the diagram shows different phases present at different compositions and temperatures. It confirmed that for Cu-rich composition, a mixed phase of Cu_2S and CIS usually exists, and for indium-rich composition, a mixed phase of $CuIn_5S_8$ and CIS were most common. As a result, it has been agreed that the

reaction between Cu_2S and In_2S_3 is the kinetic path of the CIS formation and the quasi-binary phase diagram between Cu_2S and In_2S_3 has been used to understand the equilibrium phase transformation in Cu-In-S system as explained in the following section.

2.5.2 Quasi-binary phase diagram of Cu_2S-In_2S_3

The phase diagram of the quasi-binary system, Cu_2S-In_2S_3 is given in Fig. 2.7 [34]. All compounds occurring in this system are summarized in Table 2.1.

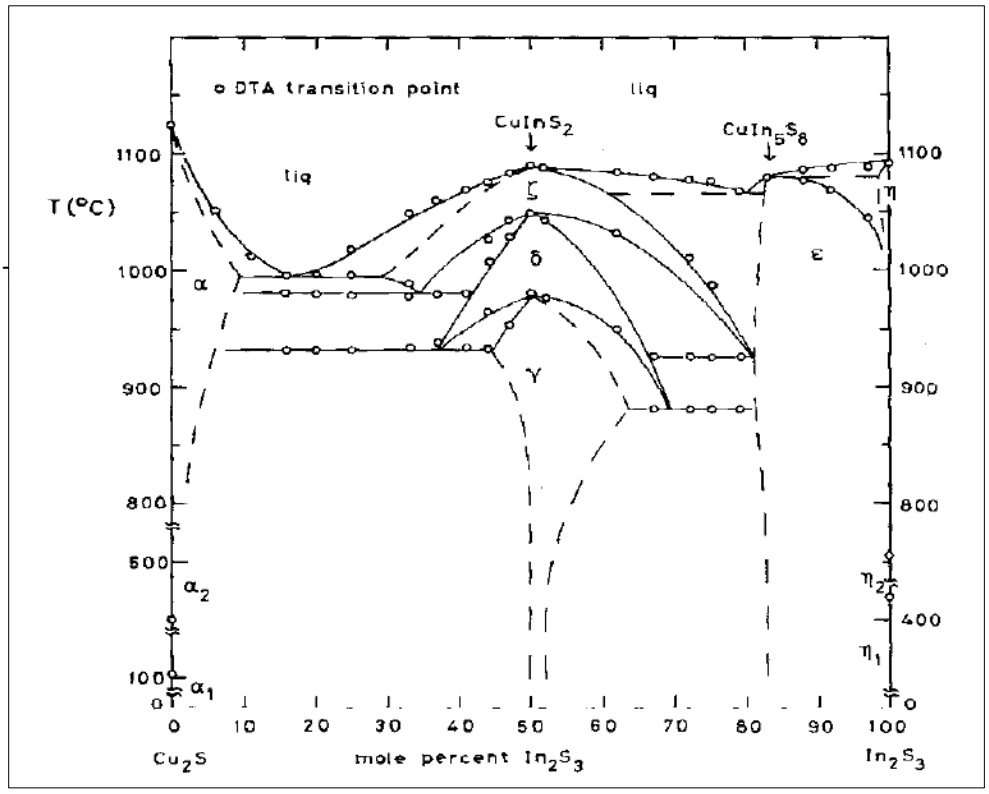

Fig 2.7 Quasi-binary phase diagram of Cu_2S-In_2S_3 [34].

Table 2.1 Compounds occurring in the system, Cu_2S-In_2S_3 with all the polymorphs and their transition temperatures.

Compound	Polymorphs	Transition temperature
Cu_2S	α_1 tetragonal	104℃
	α_2 hexagonal	450℃
	α cubic	1125℃ (m.p)
$CuInS_2$	γ chalcopyrite	980℃
	δ zincblende	1045℃
	ξ wurtzite	1090℃ (m.p.)
$CuIn_5S_8$	ε spinel	1085℃ (m.p)
In_2S_3	$\square_1$ defect-spinel	420℃
	$\square_2$ superstructure	755℃
	η_3 defect-spinel-structure	1090℃
	η layered structure	

Two semiconducting phases, CIS and $CuIn_5S_8$ appear in the diagram. $CuInS_2$ exists in three polymorphs - chalcopyrite structure up to 980 ℃, zincblende structure between 980 ℃ and 1045 ℃, and possibly wurtzite structure between 1045 ℃ and 1090 ℃ [34]. The wurtzite phase melts at 1090 ℃ and its clear identity has not been revealed yet. The second In-rich semiconductor phase, $CuIn_5S_8$ has the spinel structure over the whole temperature range from 20 ℃ to its melting point at 1085 ℃.

2.5.3 In-situ phase transition study on $CuInS_2$ thin-films

Fig. 2.8 shows the real-time investigation on the rapid thermal sulfurization of Cu-rich Cu-In alloy thin film [35]. Cu-rich case has been only studied in-situ in the literature because the field has experienced that only Cu-rich composition was able to create a device-quality CIS

layer. From room temperature to ~ 180 ℃, the sample was mainly constituted of Cu and $CuIn_2$. Before any sulfide started forming, $Cu_{11}In_9$ phase formed first during ramping. This copper enrichment of the top intermetallic phase must happen through the out-diffusion of In from $CuIn_2$ rather than the in-diffusion of Cu from Cu phase, which is confirmed by the constant Cu (200) signal - no underlying Cu was consumed to support the composition change. Since no In reflection is visible, it is assumed that the free In was liquid. $Cu_{11}In_9$ was the richest Cu-intermetallic phase observed up to ~ 330 ℃ although $Cu_{16}In_9$ was postulated as the only final intermetallic phase in the previous section – no diffraction was observed in this rapid-thermal annealing case.

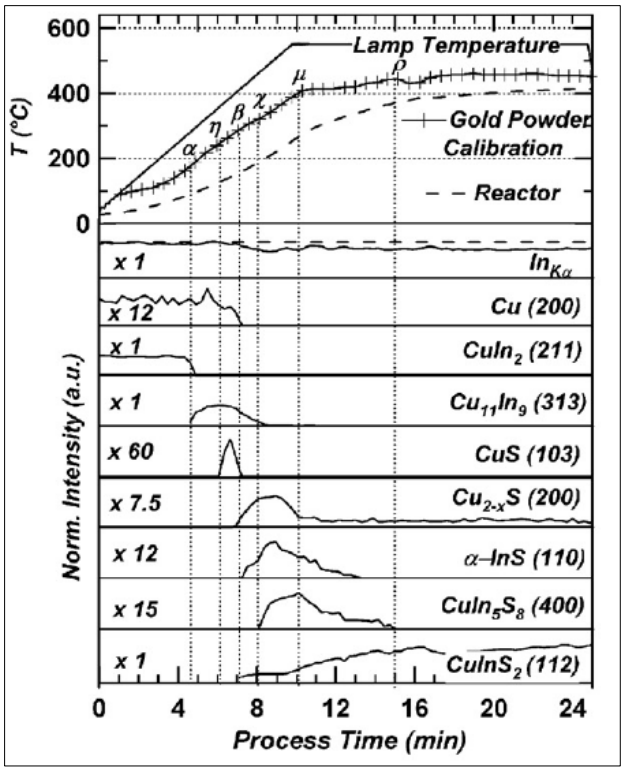

Fig 2.8 In-situ energy dispersive X-ray diffraction spectra: sulfurization of Cu-In alloy layer (Cu/In = 1.8) [35]

At about 240 ℃, CuS formed. This phase was believed to form at the top of the film where the out-coming Cu ions react with the adsorbed S atoms. From the experiment, it was

concluded that the source of Cu cation was the underlying Cu film. At about 286℃, CIS, $Cu_{2-x}S$, and InS appeared at the expense of Cu and $Cu_{11}In_9$, and the transition of CuS to $Cu_{2-x}S$ took place. Between 286 ℃ and 320 ℃, the main phases w ere $Cu_{11}In_9$, CIS, $Cu_{2-x}S$ and α-InS. The presence of InS is fundamentally different from the observations reported by Klopmann *et al* [35] - there were no signature of any In-binary phase for the sulfurization of Cu-rich films.

At ~ 320 ℃, a new phase emerged showing a spinel struc ture. Its intensity was low but increased until ~ 408 ℃. The diffraction pattern of this phase fits well to both $CuIn_5S_8$ and In_2S_3. Both phases have similar crystal structures, their main difference being the occupation of tetrahedral coordinated sites by both Cu and In cations for $CuIn_5S_8$. It was not possible to rule out a phase mixing. However, earlier thermodynamical calculations showed that the In_2S_3 cannot coexist with $CuInS_2$. The observed diffraction lines were therefore assigned to the ternary $CuIn_5S_8$ phase. From ~ 408 ℃, the signal of the existing $CuInS_2$ increased and the decrease of InS and $CuIn_5S_8$ was observed, while the $Cu_{2-x}S$ remained constant. From ~ 445 ℃, only CIS and $Cu_{2-x}S$ diffraction lines were present. A final phase transition occurred during the cool down period and it involved the copper sulfide phase segregated at the film surface. At ~ 244 ℃, the cubic digenite $Cu_{2-x}S$ phase transformed to the S-poor hexagonal b-chalcocite phase.

CHAPTER 3

EXPERIMENTAL SETUP

First, the thermal characterization of thioacetamide has been made using differential scanning calorimetry (DSC) and thermal gravimetric analysis (TGA) at Korea University through collaboration. For the metallic precursor layers, Cu and In were deposited in a sequential manner on glass substrate using a thermal evaporator. Here, we have prepared 5 different types of Cu/In atomic ratios varying from In-rich to Cu-rich compositions (Fig. 3.1). Once the film was sulfurized in a home-made reactor, the films were analyzed using scanning electron microscopy (SEM), X-ray Diffraction (XRD) and energy dispersive spectroscopy (EDS) to know the properties of the films. The study allows to learn how the composition of the Cu-In precursor layer affects the morphology and microstructure of the final compound upon sulfurization.

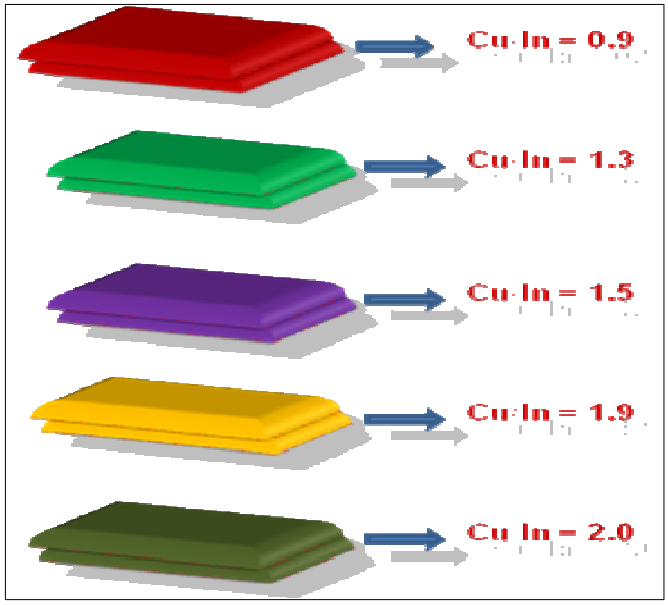

Fig 3.1 Cu-In alloy ratio layers prepared at different Cu/In ratios.

3.1 Cu-In Alloy Layer Deposition

Before the deposition of the Cu-In alloy layer, the glass substrate was cleaned with following procedure. The soda lime glass used for microscope was cut into 1 x 1 inches and was cleaned inside an ultrasonic bath with four different solvents starting from aqueous soap solution, toluene, acetone, and isopropyl alcohol. The deposition rate of the Cu-In layer in a NRC thermal evaporator was about 1 ~ 2 Å/sec (Fig 3.2). The base pressure was around 6 x 10^{-6} torr. Once the samples are deposited by the thermal evaporator, they are then sulphurized using a sulfurization set-up made in the lab.

Fig 3.2 NRC thermal evaporator.

3.2 Sulfurization Setup

In order to sulfurize the Cu-In alloy thin-film samples, a new home made reactor was built as shown in Fig 3.3.

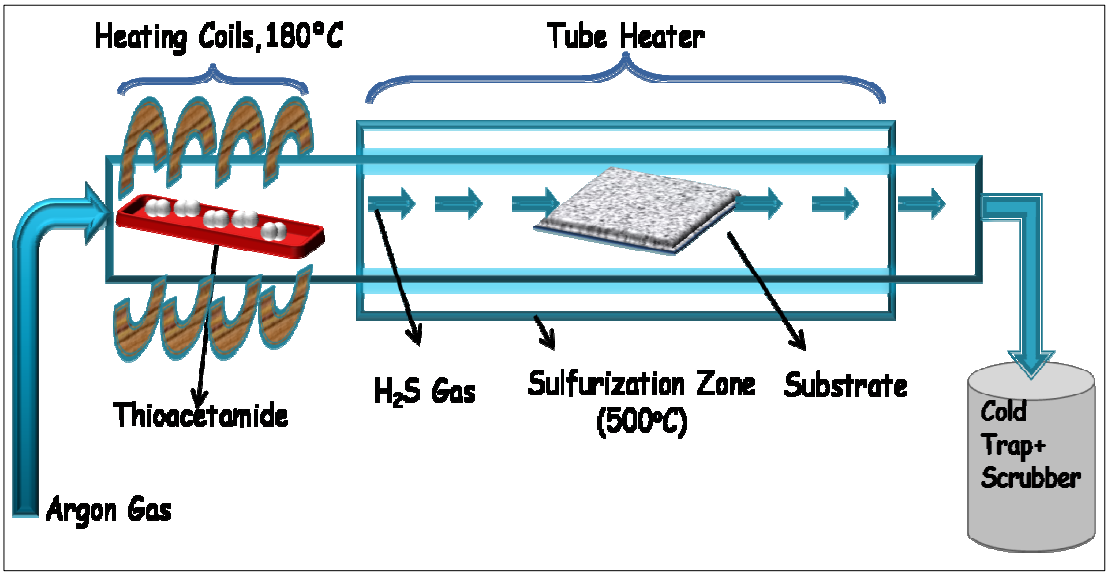

Fig 3.3 Schematic diagram of sulfurization setup.

The home made sulfurization setup was divided into two zones. The first zone shown in the figure contains a glass tube with heating coils and the second zone contains a high-temperature tube heater, where the sample was kept inside. In the first zone, 6 g of the source (thioacetamide) was kept inside a Mo boat and its temperature was monitored with a thermocouple placed between coil and the glass tube. The temperature of the coil was set to reach 180°C in about 20 minutes based on the thermal properties of the source presented in Chapter 3 - the temperature was chosen because the decomposition temperature of thioacetamide was around 180°C. When the source reaches the decomposing temperature, it is expected to decompose into H_2S and acetonitirile. They are then carried by an argon gas which acts as a carrier gas. Finally H_2S passes through the tube heater which contains the sample to be sulfurized.

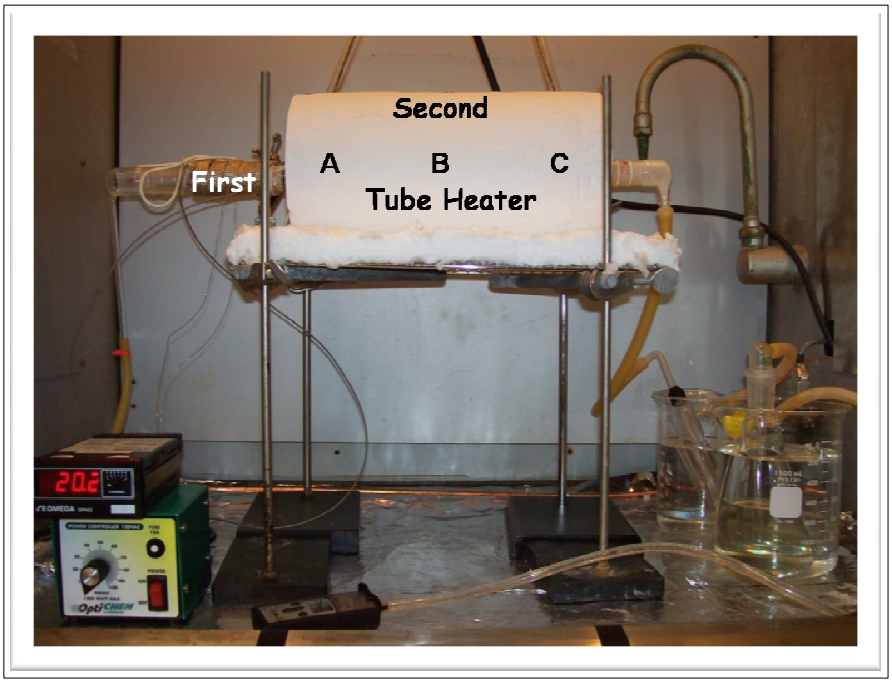

Fig 3.4 Sulfurization setup showing its tube heater.

The tube heater was purchased from Zircar (Fig 3.4). It is 24 inch long, has an inner diameter of 10 inches, and an outer diameter of 24 inches. A thermocouple was placed inside the tube heater. The temperature calibration of the tube heater was performed and it was confirmed that Zone A and Zone C maintained the same temperature, but Zone B was 100 $^{\circ}$C higher compared to Zones A and C. The Cu-In samples were kept in Zone B which was around 500 $^{\circ}$C, which was the maximum temperature during sulfurization. The temperature of Zone B was only monitored during the real operation.

Before powering the source and the tube heaters, the whole reactor was purged with Ar for 30 minutes. The power was turned on for both the source and the tube heaters at the same time. The source and the tube heater temperatures reached respectively at 180 $^{\circ}$C and 500 $^{\circ}$C in 20 minutes and were kept constant for the next 70 min. The typical temperature profiles of the source and the tube heaters are shown in Figs 3.5 and 3.6 respectively. The Ar flow rate

was controlled by a mass flow controller (MKS) and its value was set to 30 sccm throughout the experiment.

In order to collect decomposed acetonitrile, a cold trap was maintained at low temperature by ice - the gas phase of acetonitrile generated from the decomposition of thioacetamide changes to a liquid phase in the cold trap. In this experiment, we should be very careful about the toxicity of H_2S. In order to scrub any residual H_2S exhausted from the reactor, the exhausted gas was finally let through three flasks containing sodium hydroxide (6 M) in series (Fig 3.7). Finally, at the end of the third flask, a H_2S gas monitor was placed to alert if the H_2S gas reaches a dangerous level.

After 90 minutes from the beginning of the process, the process was stopped. It took another 4 hours for the system to reach the room temperature. After the samples were sulfurized, SEM and EDS were used to study film morphology and composition. XRD was also performed to study the various phases formed in the film.

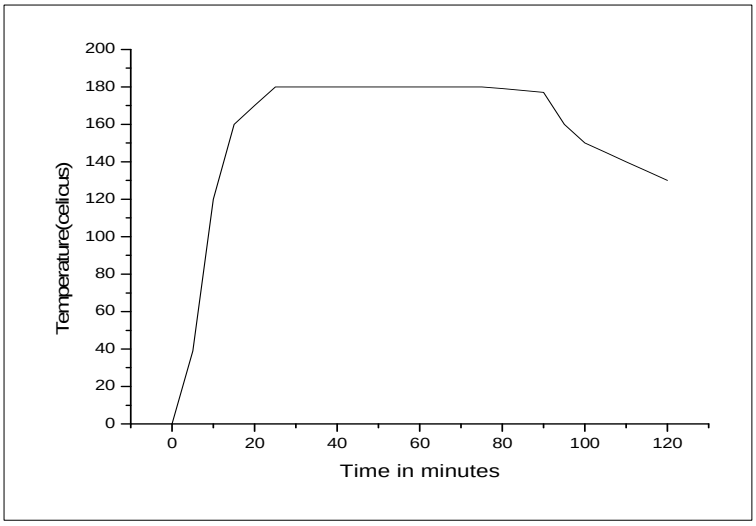

Fig 3.5 Temperature profile of thioacetamide used as a sulfur source during the sulfurization of Cu-In precursor thin-films.

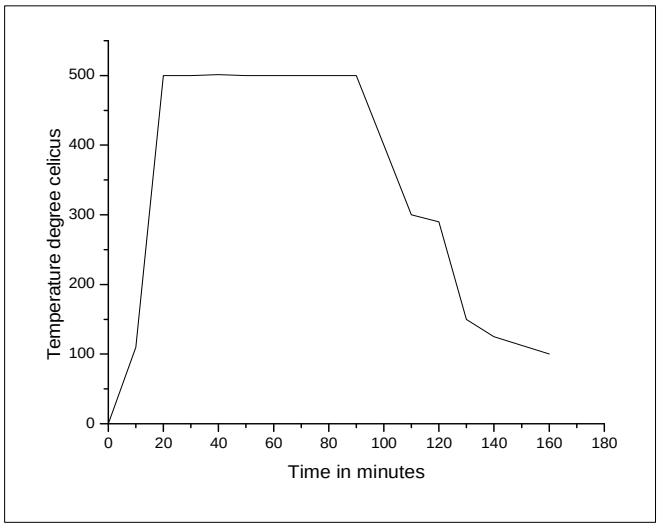

Fig 3.6 Temperature profile of the substrate during the sulfurization of Cu-In alloy thin-films.

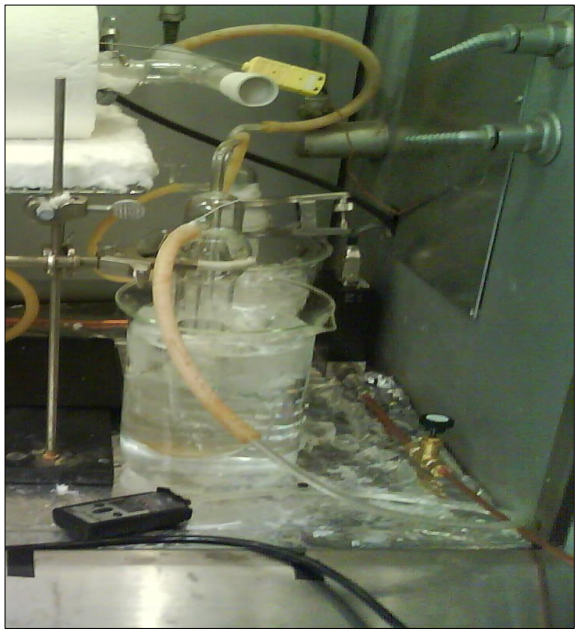

Fig 3.7 Scrubbing and monitor system for H_2S exhausted from the sulfurization setup.

3.3. Characterization Tools

This section discusses about various characterization tools that have been employed in this work.

3.3.1 KLA Tencor profilometer

Fig 3.8 KLA Tencor profilometer with 400 micron vertical range.

A profilometer (Fig. 3.8) measures the vertical depth of a material across a specified horizontal scan length. The profile is displayed on a printable graphical interface. Usage for this equipment includes measuring an etch depth, film thickness, and surface roughness. It consists of a stylus which is used to scan the surface of the film. When the stylus is moved vertically, the computer will record the movement of the stylus with respect to its penetration depth. This instrument has been used to measure thicknesses of the films in this study.

3.3.2 Scanning electron microscopy

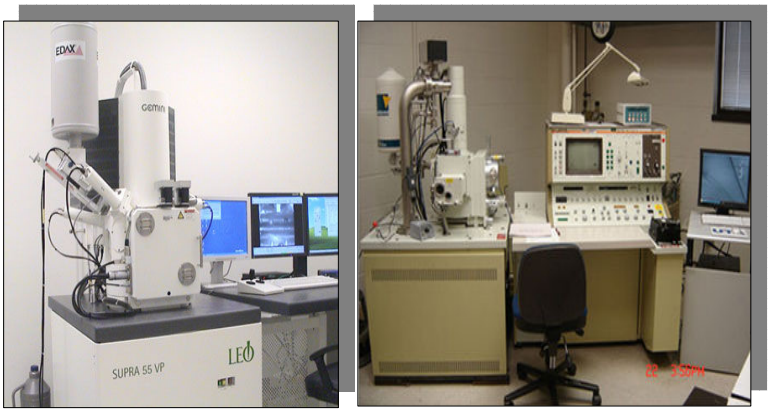

Fig 3.9 SEM- ZEISS Supra 55 VP (left) and JEOL JEM 845 SEM (right).

SEM (Fig. 3.9) is a type of an electron microscope that images the sample surface by scanning it with a high-energy beam of electrons; the electrons interact with the atoms that make up the sample producing signals that contain information about the sample's surface topography and composition of the sample, which can be measured by the EDS detector attached to SEM.

3.3.3 Four- point probe method

Fig 3.10 FPP-5000 four-point probe.

Four-point probe (Fig. 3.10) measures the sheet resistance of the sample. There are four probes - the known current is passed between the outer two probes, and the voltage drop is measured across the two inner probes.

3.3.4 X-ray diffraction

Fig 3.11 D-500 X-ray diffractometer.

X-ray diffraction (Fig. 3.11) is a technique to measure the crystallinity of the thin films, size of the grains, and phases in the materials. When fast moving electrons strike the metal target, X-ray is produced. This high energy X-ray will be diffracted at the sample providing a diffraction pattern. In this work, this equipment has been used to identify the various phases present in the film. It has also been used to find the relative crystallinity of the phases.

3.3.5 RF/DC magnetron sputtering

Fig 3.12 Magnetron sputter.

Sputtering (Fig. 3.12) is the technique used to deposit films on the surface of the substrate. This process occurs by bombarding the surface of the target by gaseous ions generated under high potential. Inside the sputter chamber, there are a target and a substrate which often act as a cathode and an anode respectively. Applying a voltage to the cathode and anode develops an electric filed between them. When an inert gas like Ar passes inside the chamber, it gets ionized by the electric field and the ions hit the target with high energy. The sputtered atoms, molecules, ions, and radicals reach the substrate and this leads to the deposition of thin film on the substrate. This equipment has primarily been used for the deposition of ITO on top of CdS during the fabrication of the solar cells. Typical condition of the deposition is summarized in Table 3.1 and the thickness of the ITO film was around 500 nm.

Table 3.1 Sputtering parameter for the deposition of ITO.

Deposition rate	2 Å/sec
Power	100 W
Time	45 min

3.3.6 UV-Visible NIR spectroscopy

Spectroscopy is a branch of science in which light is used to study the structure of matter and used to carry out qualitative and quantitative analysis. It is also used for the identification ofsubstances from the spectrum emitted or absorbed by the substances. In this study, absorbance and % transmittance was carried out using a Perkin Elmer UV-Visible-NIR. Spectrometer Lambda 19 unit (Figure 3.1.3).

Figure 3.13 Perkin Elmer UV-Visible-NIR Spectroscopic unit.

3.3.7 I/V Measurements

Characterizing CIS solar cell was carried out under AM 1.0 condition using a home-built solar simulator equipped with Keithley 2420 3A source measurement unit. Projector lamp purchased from GE lighting General was used as a light source and GaAs single junction solar cell donated by NASA Glenn Research Center was used to calibrate the lamp to AM 1.0.

CHAPTER 4

RESULTS AND DISCUSSION

4.1 Thermal Characterization of Thioacetamide

Thermal properties of thioacetamide were analyzed by using DSC first. A calorimeter is an instrument used to measures the heat flow involved in the chemical reactions with respect to a reference sample. The main applications of DSC in this work are to study the phase transitions of thioacetamide such as melting and decomposition. These transitions involve energy changes that can be detected by DSC with great sensitivity. These measurements provide information about physical and chemical changes of thioacetamide.

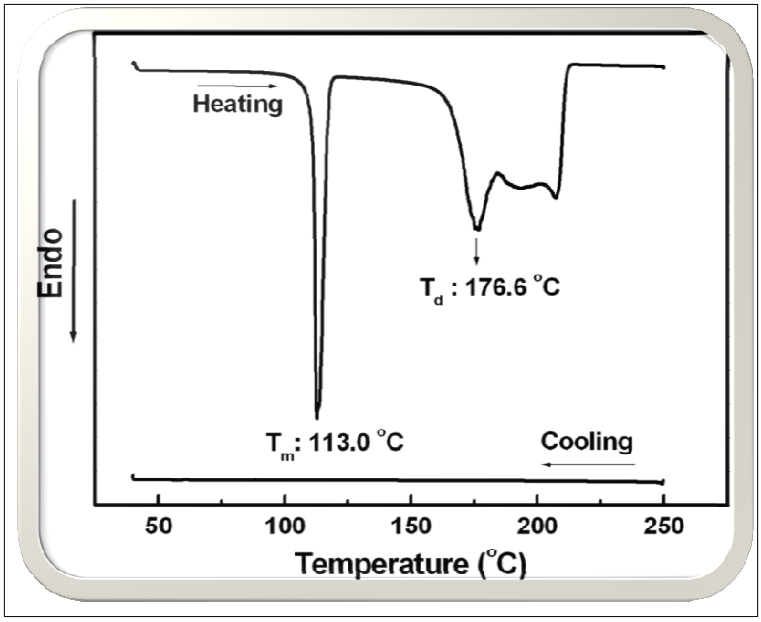

Fig 4.1 DSC characterization of thiaoacetamide.

The results obtained were shown in Fig 4.1. Thioacetamide experienced an endothermic reaction signatured by the presence of a downward peak at 113 °C. This means the heat was absorbed by the thioacetamide and it is assigned to its melting. After increasing the temperature from its melting point, there was a sudden drop at 176.6°C which indicates that thioacetamide was decomposing. Upon decomposition, thioacetamide is expected to give out H_2S and acetonitrile as discussed in previous chapters. In fact, the cooling curve in the bottom of the figure indicates the process was irreversible suggesting its decomposition.

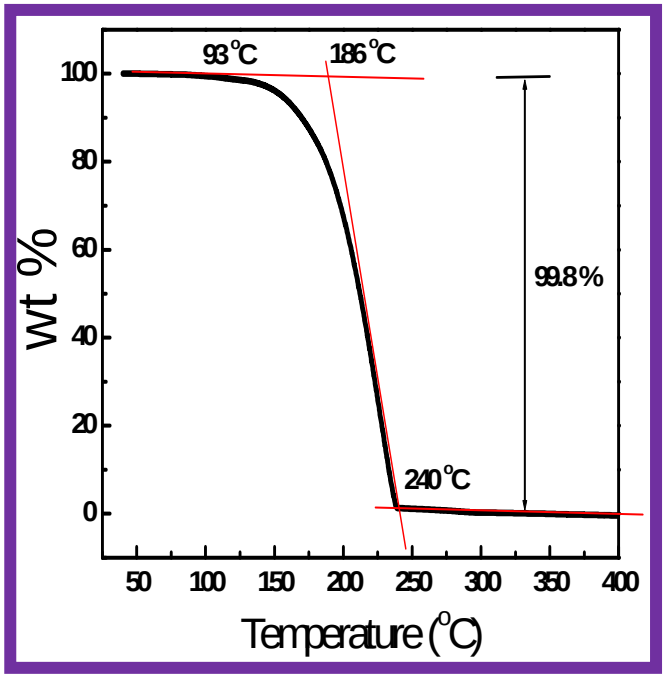

Fig 4.2 TGA characterization of thioacetamide; weight loss as a function of temperature.

The measurement was further carried out using TGA as shown in Fig 4.2, which gives the weight loss of a sample as a function of temperature or time. It was performed over a temperature range from 50 ℃ to 400 ℃ and the heat ing rate of 10 ℃/min was automatically regulated by the instrument. Initial sample weight was 46.6 mg and the measurement was carried out under nitrogen atmosphere with a N_2 flow rate of 150 cc/min. At 186 °C, there was sudden decrease in weight, which indicated that there was material loss for thioacetamide upon its decomposition according to the previous DSC analysis - the transition from one material to

another is typically indicated by weight loss versus temperature curve and a peak from DSC plot.

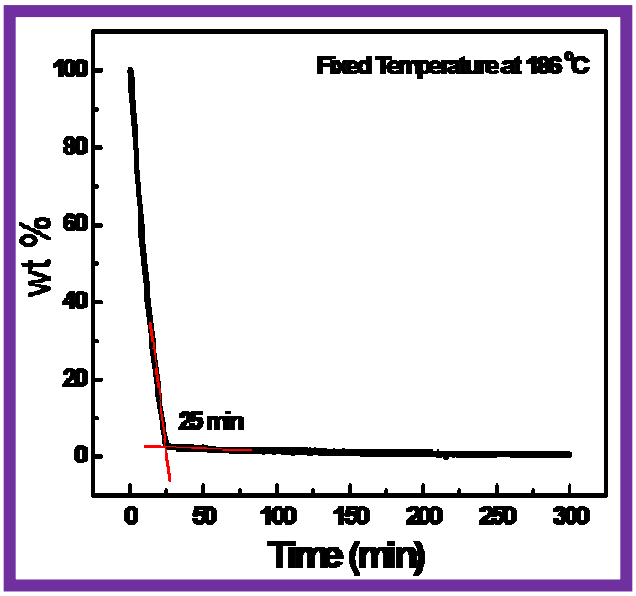

Fig 4.3 TGA characterization of thioacetamide; weight loss as a function of time at a fixed temperature.

A graph is plotted between wt% loss and time and keeping the temperature constant at 186 °C (Fig. 4.3). The figure shows that as soon as the process starts, thioacetamide starts decomposing, and all the byproducts have been purged out of the TGA system in 25 minutes. The data helped in optimizing the sulfurization process when thioacetamide is used as a source of sulfur in the process

4.2 Phase Analysis of Cu-In Alloy Thin films

Fig. 4.4 shows XRD patterns collected for Cu-In alloy thin-films on glass with five different Cu/In ratios. The patterns show how the phases changes with respect to the [Cu]/[In] ratio. For the In-rich films, we can see strong presence of In peak at 2θ of 33 degree and diffraction peaks associated with $Cu_{11}In_9$. Furthermore, most In-rich film (Cu/In = 0.9) did not show any signature of Cu peak at all while Cu-rich films always contained elemental Cu. For

Cu-rich films, dominant phases include Cu and $Cu_{16}In_9$. The presence of $Cu_{16}In_9$ can be expected from the Cu-In phase diagram shown in chapter 1 [24].

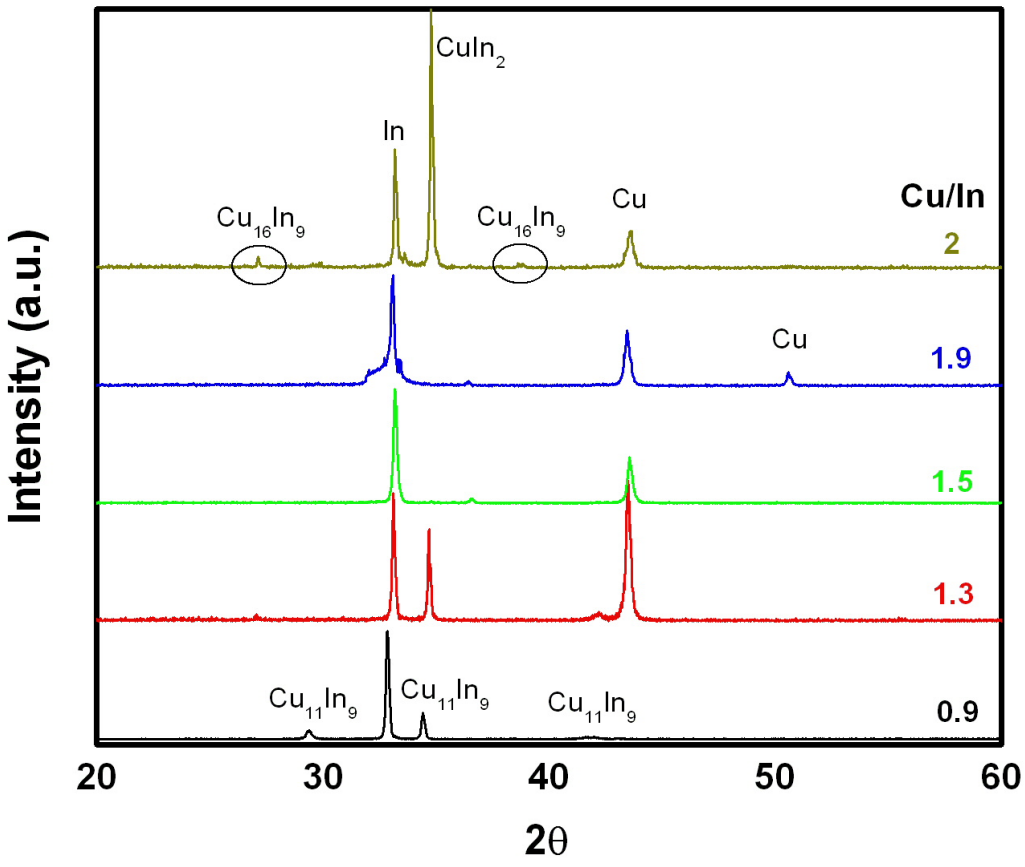

Fig 4.4 XRD analysis of Cu-In precursor thin-films.

4.3 Phase and Micro structural Analysis of $CuInS_2$ Thin Films

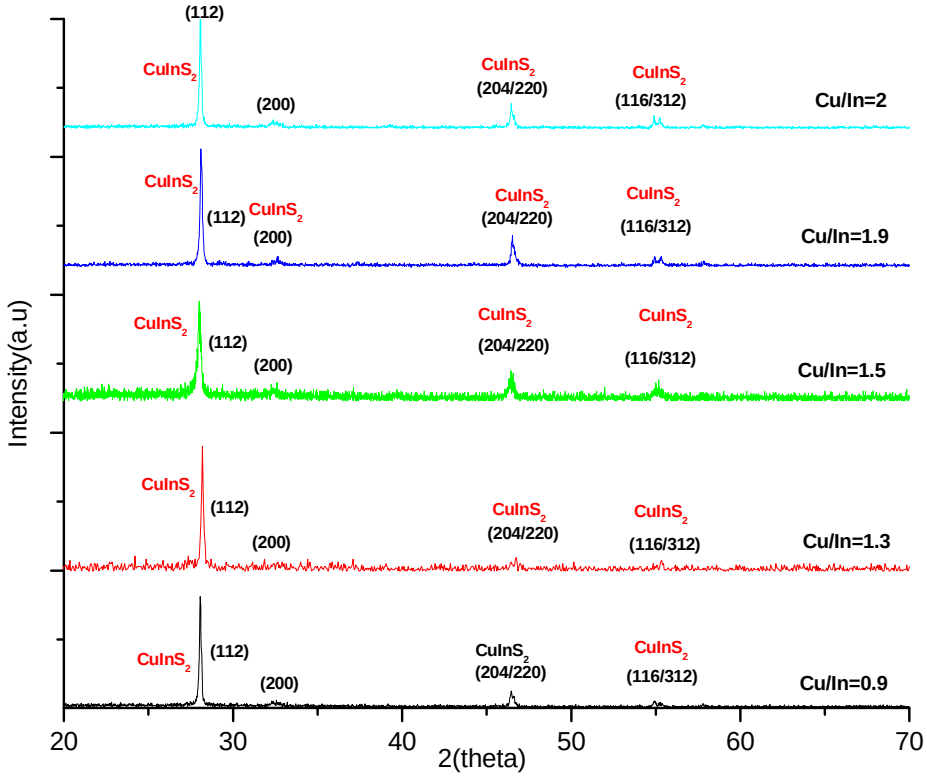

Fig 4.5 XRD patterns of $CuInS_2$ thin-films from the sulfurization of Cu-In layers.

The structural properties of the sulfurized films were investigated using XRD measurement as shown in Fig 4.5. The figure provides the comparison of XRD spectra from sulfurized thin films with different Cu/In ratios and the data were normalized to the intensity of (112) peak in the film with Cu/In = 2.0. Their chalcopyrite structure was confirmed by search-matching their diffraction patterns with reference patterns from Joint Committee on Powder Diffraction Standards (JCPDS) of the International Center for Diffraction Data (ICDD). The reference pattern # 750106 matches well with the measured diffraction patterns.

The coherence length, which is an indicator of the quality of the crystalline phase was calculated using XRD data for the films and it was summarized in Table 4.1. The coherence length can be calculated by using a Scherrer's formula [36],

$$T = (0.9 \times \lambda) / \{B \times \cos(\theta_B)\}$$

where,

T is the coherence length in nm,

λ is the wavelength of the X-rays in nm ($\lambda \cong 0.154$ nm for Cu K_α source),

B is the full width half maximum (FWHM) in radian, and

θ_B is the Bragg angle in degree ($\theta_B = 14°$ was used for (112) plane in this study.)

The FWHM refers to the extra breadth or broadening due to the disorder in the crystal.

Table 4.1: Coherence length related to Cu/In ratio.

Cu/In ratio	FWHM (radian)	Coherence length (nm)
0.9	0.00262	55
1.3	0.00332	43
1.5	0.00262	55
1.9	0.00253	56
2.0	0.00244	58

The table shows that as Cu/In ratio increased, the coherence length has increased from 43 nm to 58 nm for Cu-rich films, which was reflected in the decrease in FWHM of (112) peak as Cu/In ration increases. In the meantime, the coherence length was suddenly increased by changing from Cu-rich composition to In-rich composition, which is not well understood at this moment and requires further study. Further discussion will be made together with the morphological analysis of the films made by SEM in section 4.5.

4.4 Compositional Analysis of $CuInS_2$ Thin Films

The compositional analysis of the sulfurized samples is given along with the initial Cu/In ratio before sulfurization as shown in Figs. 4.6 and 4.7. During sulfurization process, Cu/In ratio

increased from the initial ratios as seen from Fig 4.6, which is assigned to the result of In loss during sulfurization process.

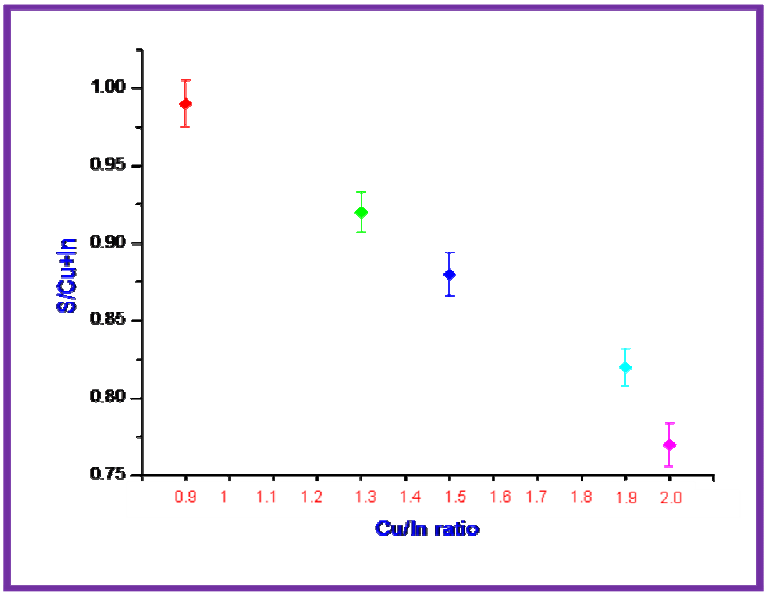

Fig 4.6 Cu/In ratio of $CuInS_2$ thin-films after sulfurization versus Cu/In ratio in Cu-In alloy thin-films.

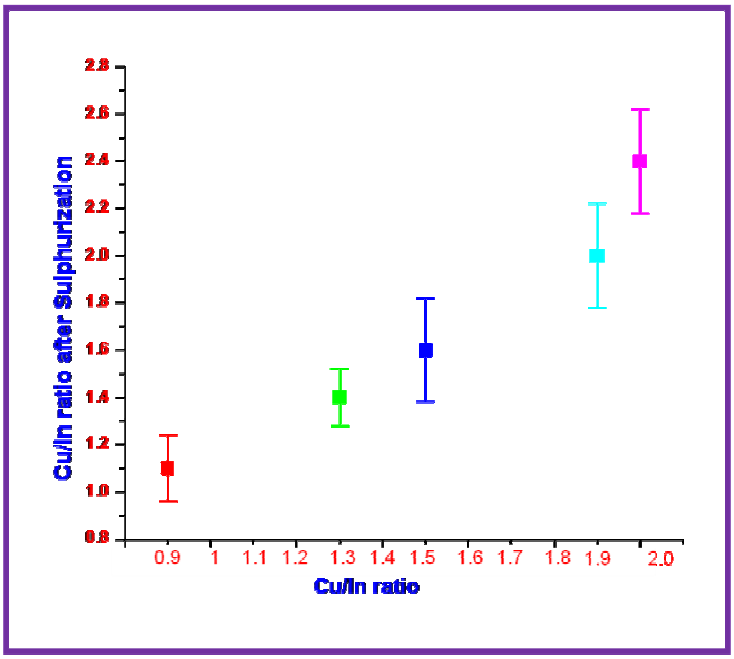

Fig 4.7 S/(Cu+In) ratio versus Cu/In ratio of $CuInS_2$ thin-films after sulfurization.

The S/(Cu+In) ratio needs to be 1.0 in order to become a stoichiometric CIS composition. But in Fig 3.7, we see the stoichiometric ratio is between 0.7 and 0.9, which indicates that we are not attaining the desired stoichiometric ratio. The sulfur deficiency in the films can be explained either by the presence of a secondary phase, Cu_xS ($x > 1$) or the decrease in the reactivity of the film as the Cu/In ratio increases. In order to confirm the possible presence of the secondary phase, Cu_xS, the $CuInS_2$ films were etched using KCN because Cu_xS is expected on the surface of the film and its removal can be reflected in the change of Cu/In ratio upon etching. But the thin films were all peeled off from the substrate, which indicates that Cu_xS phase may be present underneath $CuInS_2$ film possibly in addition to other area in the film. However, XRD and EDS could not confirm the presence of Cu_xS phases within their sensitivities, which is not uncommon in the field.

4.5. Morphology of $CuInS_2$ Thin Films

The surface morphology and microstructure of the $CuInS_2$ films on glass made in sulfur atmosphere at 500℃ were studied by SEM and presented in Figs 4.8 to 4.9. The surface morphology of the CIS films was found to be very sensitive to the Cu/In ratio. Generally, the

figures showed that the increase in Cu concentration in the film produces bigger grains – this can be also correlated with coherence length calculated in section 4.3. This is because, in Cu-rich films, Cu_xS phase will be formed on the surface of the film – also possibly in other area in the film as seen from the KCN etching experiment- and it will acts as a flux to grow larger and better $CuInS_2$ grains [31]. The mismatch between coherence length and the grain size observed in the SEM pictures is possibly due to the fact that the grains are highly defective. While In-rich films have tetragonal bisphenoids as seen from the figure, Cu-rich films show more equiaxed grains. While the consideration of surface energy predicts the tetragonal bipyramid grains, non-equilibrium anisotropic growth in [221] directions – normal to (112) plane - can promote tetragonal bisphenoid grains as shown in Fig. 3.10 [30]. The presence of Cu_xS as a liquid phase in Cu-rich films is expected to lead an equilibrium grain growth in the $CuInS_2$ producing more equiaxed grains (tetragonal bipyramid grains).

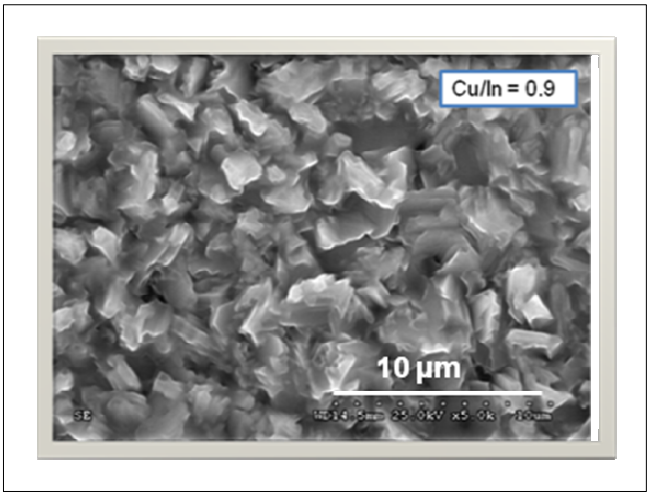

Fig 4.8 SEM image of In-rich $CuInS_2$ thin film

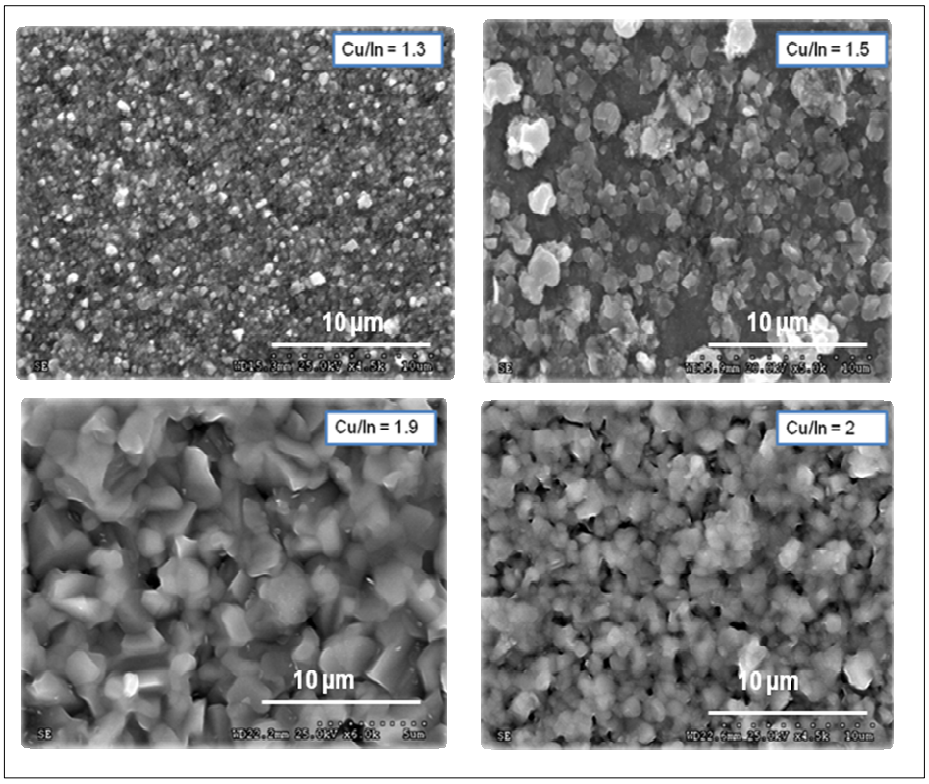

Fig 4.9 SEM images of Cu-rich $CuInS_2$ thin film.

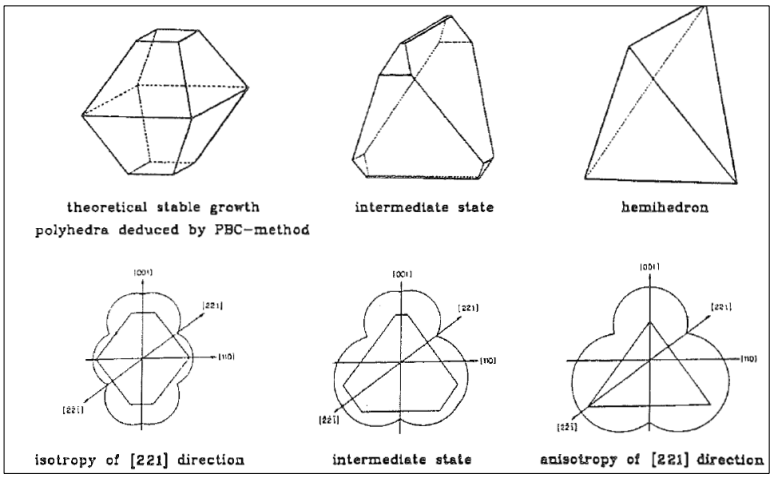

Fig 4.10 The shapes of the chalcopyrite crystals based on the surface energy consideration [37].

Fig. 4.11 shows the clearest In-rich morphology observed from an In-rich film (Cu/In = 0.9), which was made during the optimization process of reactor – this particular sample is not a part of the batch of samples covered in this thesis. While it was unfortunate that author could not reproduce the similar morphology again, the figure clearly shows the (112) triangular faces of tetragonal bisphenoid grains - circle in the picture in particular. Assuming CIS tetragonal structure does not have any tetragonal distortion, (112) face is expected to be an equilateral triangle and in fact the triangle in the circle is quite close being equilateral.

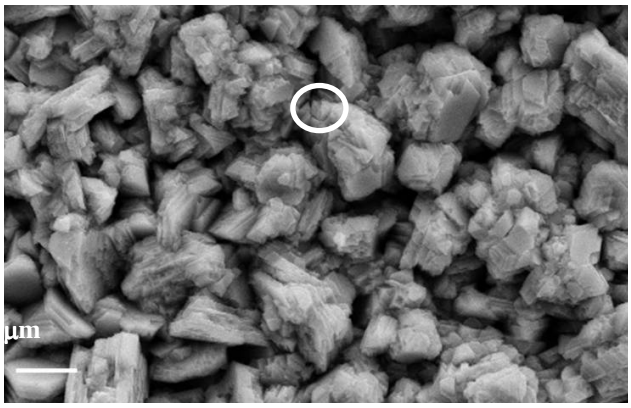

Fig. 4.11 Tetragonal bisphenoid grains with equilateral triangular (112) faces observed in In-rich CIS film.

4.6 Optical Properties of $CuInS_2$ Thin Films

Fig 4.12 shows that at different Cu/In ratios, there is a change in the optical bandgap and it can be explained by the change in the density of defects around band edges, which can be predicted from the grain size and coherence length in a rough sense. The figure indicated that as Cu/In ratio increases, the films have higher band gap for Cu-rich films. Larger grains with longer coherence length possibly mean fewer defects in the grains when compared to smaller grains. Density of states at the band edges will be more for smaller grains when compared to larger grains. While it is not clear why In-rich film have large grains suddenly, its optical bandgap is certainly larger than any other Cu-rich films with shorter coherence length.

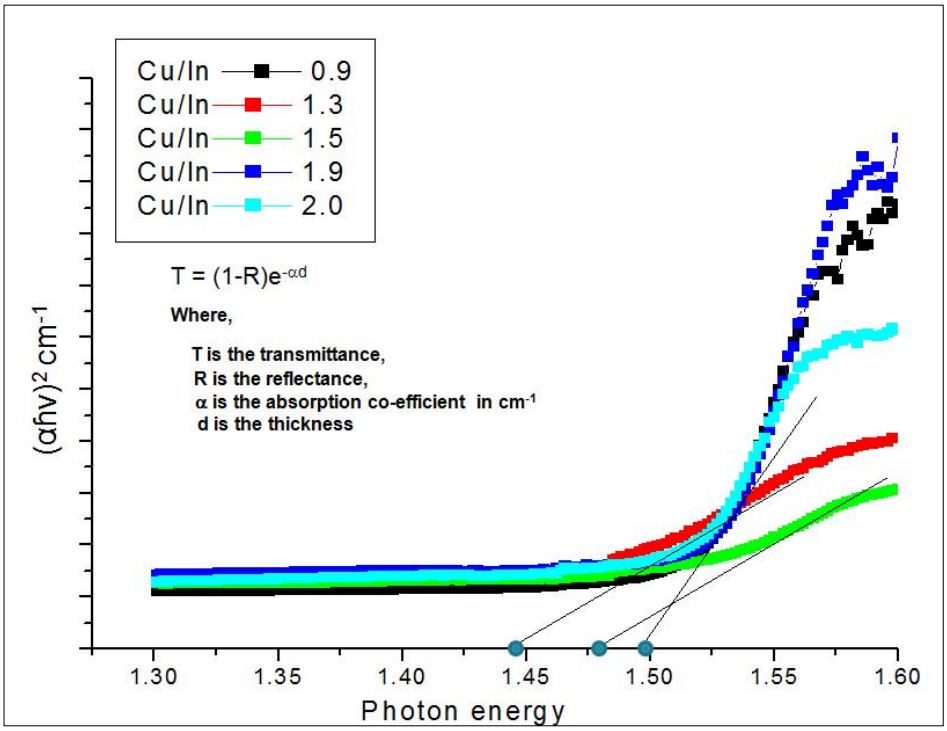

Fig 4.12 Absorption coefficient (α) and optical band gap of $CuInS_2$ at different ratios

4.7 Cell Measurements

A batch of CIS/CdS single-heterojunction solar cells were fabricated with a series of CIS absorber layers that have different Cu/In ratios. The cells were fabricated with a structure of Al/ITO/CdS/CIS/Mo. While most CIS thin-films have peeled off during CdS deposition, the absorber device with Cu/In=1.3 seemed fine enough for further fabrication. Fig. 4.13 shows its output characteristics. Very low open circuit voltage does not allow detailed analysis of the device and it is necessary for further optimization. Yet, photovoltaic effect was successfully observed from the device.

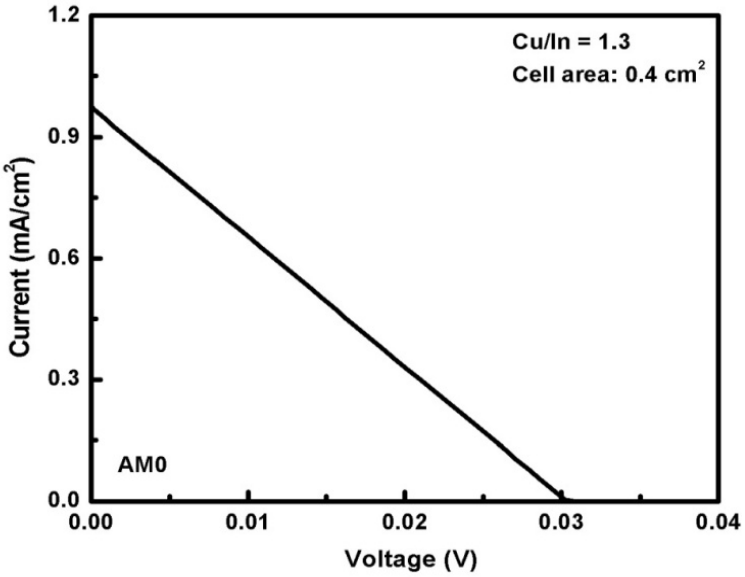

Figure 4.13 I-V characteristics of a $CuInS_2$ solar cell made with thioacetamide (Cu/In = 1.3).

CHAPTER 5

CONCLUSION

In this research, a novel method for sulphurization of Cu-In alloy using thioacetamide as a sulphurization source was studied. The thermal stability of thioacetamide has been investigated by using DSC and TGA, and the decomposition temperature of thioacetamide was found to be at around 180 °C producing hydrogen sulfide. Cu/In precursors with different Cu/In ratios were first prepared by thermal evaporation of copper and indium using a thermal evaporator, and then used as the precursor for sulphurization. The sulpurization was done in a quartz tube reactor. The formation of a chalcopyrite structure at the different ratios was analyzed by using XRD, SEM and EDS. The analysis has concluded that copper rich films have larger grains than those from copper poor films. This is due to the presence of CuS in copper rich films. It will act as a flux to grow larger grains in copper rich films. The optical properties of $CuInS_2$ were finally discussed and the results explain that the optical band gap of $CuInS_2$ thin films varies with respect to Cu/In ratio. Larger grains – possibly meaning better crystalline structure - have fewer defects when compared to smaller grains. Density of states will be more for smaller grains due to presence of defects, when compared to larger grains. This leads to change in the energy gap from copper poor to copper rich films.

REFERENCES

1. M. Krunks, A. Mere, A. Katerski, V. Mikli, and J. Krustok, “Characterization of sprayed $CuInS_2$ films annealed in hydrogen sulfide atmosphere”, Thin Solid Films, 511, 26 (2006).
2. Kai Siemer, Jo Klaer, Ilka Luck, Jürgen Bruns, Reiner Klenk, and Dieter Braünig, “Efficient CuInS2 solar cells from a rapid thermal process (RTP)”, Solar Energy Materials & Solar Cells 67, 159 (2001).
3. Rajalakshmi Sundaramoorthy, Karan Agrawal, and Michael H.-C. Jin, Proceedings of the 33rd IEEE Photovoltaic Specialists Conference (San Diego, 2008).
4. Chopra, K. L., Paulson, P. D., and Dutta, V. Progress in Photovoltaics: Research and Applications, 12, 69 (2004).
5. Braunger, d.Hariskos, D.Bilger G.Rau and Schock, H.W, “Influence of sodium and selenium incorporation on the electronic transport mechanism of Cu(In, Ga)Se_2 solar cells”. Solid state Commun, 107, 59 (2000).
6. C. D. Lokhande, A. Ennaoui, P. S. Patil, M. Giersig, K. Diesner, M. Muller, and H. Tributsch, “Chemical bath deposition of indium sulphide thin films preparation and characterization”, Thin Solid Films, 340, 18 (1999).
7. Nakada, T. and Mizutani, M., Japanese Journal of Applied Physics, 41, 165 (2002).
8. Bhattacharya, R. N. and Ramanathan, “Cu(In,Ga)Se_2 thin film solar cells with buffer layer alternative to CdS Solar Energy”, 77, 679 (2004).
9. Nakada, T. and Mizutani, M. "18% Efficiency Cd-Free Cu(In,Ga)Se_2 Thin-Film Solar Cells Fabricated Using Chemical Bath Deposition (CBD)-ZnS Buffer Layers”, Japanese Journal of Applied Physics, 41 165, (2002).
10. Bergmann, R. B., “Crystalline Si thin-film solar cells a review”, Applied Physics A, 69, 187 (1999).

11. Masayuki Tanda and Susumu Manaka,"Photoluminescence Study of $CuInSe_2$ Thin Films Prepared by the Selenization Technique", Japanese Journal Appl Phys.31, 753 (1992).
12. Neelkanth, G.Dhere and Sachin S.Kulkarni "Composition and morphology of partially selenized $CuIn_{1-X}Ga_X$ Se_2 thin films prepared using diethylselenide as selenium source", Journal of Physical and Chemistry of Solids, 66, 1876 (2005).
13. S. Bandyopadhyaya, S. Roy, S. Chaudhuri, and A. K. Pal, "$CuIn(S_XSe_{1-X})_2$ films prepared by graphite box annealing of In/Cu stacked elemental layers", Vacuum, 62, 61 (2001).
14. P. R. Subramanian and D. E. Laughlin, "The Cu-In (Copper-Indium) System, Bulletin of Alloy Phase Diagrams", 5, 554 (1989).
15. Koster, L. Wolff, and G. Visser, "Coevaporated Cu-In films as precursors for solar cells", Acta Crystallogr. Sect B, 36, 3094 (1980).
16. Practical Handbook of Photovoltaic: Fundamentals and Applications, 369 (2003).
17. Rommel Noufi and Ken Zweibel, "High-Efficiency CdTe and CIGS Thin-Film Solar Cells: Highlights and Challenges", IEEE 4^{th} Photovoltaic Conversion, 317 (2006).
18. C. Dzionk, H. Metzner, S. Hessler, and H. E. Mahnke, "Phase formation during the reactive annealing of Cu–In films in H_2S atmosphere", Thin Solid Films, 299, 38 (1997).
19. Hann, G.Jasenek, A.Hanna,G. and Schock, "Electrical characterization of $Cu(In,Ga)Se_2$ thin films solar cells and the role of defects for the device performance", Solar Energy Mater and Solar Cells, 67, 137 (2001).
20. Ruckh, M.Schmid, D.Kaiser, Influence of substrates on the electrical properties of Cu (In, $Ga)Se_2$ thin films, Proc.of the First World Conf. on Photovoltaic Solar Energy Conversion, 156 (Hawaii, 1994).
21. Keyes, B.M Hasoon, "Influence of Na on the electro-optical properties of $Cu(In,Ga)Se_2$", Proc. Of 26^{th} IEEE Photovoltaic Specialists Conf., 479 (1997).
22. Bulent M, Basol and Vijay K.Kapur, Proc. of the 21st IEEE PVSC, 546 (New York, 1990).
23. P.Villars and L.Calvert in Pearsons Handbok of Crystallographic Data for International Phases, 2, 854 (1985).

24. A. Bolcovage, S. W. Chen, C. R. Kao, Y. A. Chang, and A. D. Romig, “Phase Equuilibria of the Cu-In System”, Journal of Phase Equilibria, 14, 14 (1993).
25. T. P. Rajasekharan and K. Schubert, Z. “Crystal Structure of $Cu_{11}In_9$”, Metallkd. 72, 275 (1981).
26. J. Reynolds, W. A. Wiseman, and W. Hume-Rothery, “A thermodynamic optimization of the Cu-In system”, J. Inst. Met. 80, 637 (1951).
27. W.Keppner, T.Klas, W.Korner, R.Wesche, and G.Schatz, "Compound Formation at Cu-In Thin-Film Interfaces Detected by Perturbed γ-γ Angular Correlations", Phys.Rev .Lett.54, 2371 (1985).
28. H.S. Liu, X.J. Liu, Y. Cui, C.P. Wang, I. Ohnuma, R. Kainuma, Z.P. Jin, and K. Ishida, "'Thermodynamic Assessment of the Cu-In Binary System", Journal of Phase Equilibria and Diffusion 23, 409 (2002).
29. B.Dimmler, H.Dittrich and H.W.Schock, "Performance and Optimization of Hetrojunctions Based on Cu(Ga,In)Se_2", IEEE conference (1987).
30. H.Dittrich and H.W.Schock, "Analysis of Growth Structure of Polycrystalline Chalcogenide thin films by X- Ray Diffraction", Springer Proceedings in Physics, 54, 432 (1991).
31. 4. S.Zhang and Z.Alex,”Defects Physics of the $CuInSe_2$ chalcopyrite semiconductor”, Phy review B, 57, 16 (1998).
32. R.Klenk and H.Schock,”A model for the successful growth of Polycrystalline films of $CuInSe_2$ by mulitisource physical vacuum Evaporation”, Adv.Mater, 5, 2 (1993).
33. H. Rodriguez Alvarez,I.M. Kotschau, H.W. Schock”Pressure-dependent real time investigation on the rapid thermal sulfurization of Cu-In thin films”, Journal of Crystal Growth,3638, 310 (2008)
34. J.J.M. Binsma, L.J. Giling, and J. Bloem ” Phase Relations In The System Cu_2S-In_2S_3”J.Cryst Growth 50:429–436,1980.
35. Ch. von Klopmann, J. Djordjevic, R. Scheer, “Real-time studies of phase transformations in Cu-In-Se-S” Journal of Crystal Growth, 289, 113 (2006).

36. Elements of X- ray Diffraction, B.D.Cullity and S.R.Stock

37. Dittrich H, Schock HW. In Springer Proceedings in Physics, 54. p. 432(1991).

BIOGRAPHICAL INFORMATION

Alex Alphonse was born in Tiruchirapalli, a beautiful city from India. He finished his Master of Material Science from Anna University, Chennai, India. As a part of curriculum, he had done his project on the corrosion of 9% nickel and their properties in WRI (Welding Research Institute), BHEL, Trichy. He worked as an instructor in Mookambigai college of Engineering, Pudukkotai for one year.

In fall 2007, he joined Master of Material Science and Engineering as a graduate student at the University of Texas at Arlington. He worked as a research assistant in the Photovoltaic Materials Laboratory for 2 years. After completion his master degree, he is working in Nano-Master as a Manufacture Engineer.